



Activated carbon treated with different chemical agents for pertechnetate adsorption

Marek Hupian¹ · Michal Galamboš¹ · Eva Viglašová¹ · Oľga Rosskopfová¹ · Vipul Vilas Kusumkar¹ · Martin Daňo²

Received: 12 October 2023 / Accepted: 25 January 2024 / Published online: 27 February 2024
© The Author(s) 2024

Abstract

The study investigated the adsorption behaviour of different activated carbon samples for pertechnetate under diverse conditions. Characterizations of A-CF-F and A-CF-Z samples were done using BET, FTIR, XRD, XRF and SEM–EDX methods. In batch experiments, maximum adsorption occurred at pH 2, with a swift process and an optimal phase mixing time determined as 1 h for all of the samples. Analyzing experimental data using Langmuir and Freundlich adsorption models revealed coefficients of determination R^2 exceeding 90%. The Freundlich isotherm was found to be more suitable for describing the adsorption process.

Keywords Pertechnetate · Activated carbon · Chemical activation · Adsorption

Introduction

Activated carbon (AC) was first defined by Schanz [1] as any carbon form capable of adsorption. This material belongs to the group known as pyrogenic carbonaceous materials (PCMs), which are typically prepared through thermochemical conversion of certain precursors containing a high amount of carbon. Apart from activated carbon this group contains e.g. biochar, hydrochar or carbon nanotubes. PCMs primarily function as effective adsorbents for removing contaminants from aqueous solutions [2]. They also find applications in anaerobic reduction of azo dyes, oxidation of dyes and impurities in electrochemical wastewater treatment, as antidotes for poisoning and kidney diseases in medicine, and as decolorizing or deodorizing agents in industries, among others [3, 4]. Activated carbon (AC) is particularly noteworthy due to its properties, such as a high surface area

(600–2000 $\text{m}^2\cdot\text{g}^{-1}$), well-defined microporous structure or presence of various functional groups on its surface [5]. The mechanism of AC adsorption for the removal of organic and inorganic pollutants relies on various processes, including electrostatic interaction, ion exchange, pore filling, and precipitation. The specific mechanism is influenced by the physicochemical properties of the material, such as dosage, pyrolysis temperature, and the pH of the medium or effluent [6]. Activated carbon is prepared through pyrolysis and followed by physical or chemical activation. This activation process enhances porosity and specific surface area, thus increasing the adsorption capacity. The choice of precursor and optimization of pyrolytic and activation conditions are crucial in achieving satisfying adsorption properties [7]. Several studies used different precursors for preparation of activated carbons, e.g. from biomass, waste, plant parts [8], peanut shells [9], pineapple waste [10], oil palm shell [11] or coffee beans [12]. Most organic substances that obtain high percentage of C are potential raw materials for production of ACs. To produce a highly porous C structure, the factors of high % of C, low inorganic content, low degradation upon storage or the cost of precursors should be considered. Lignocellulosic materials are generally accepted as precursors of AC [13]. Pyrolysis is a thermochemical conversion of organic biomass to liquid or/and gaseous fuels at high temperature in the absence of oxygen and this process is irreversible [14]. After pyrolysis, the material undergoes

✉ Marek Hupian
marek.hupian@uniba.sk

¹ Department of Nuclear Chemistry, Faculty of Natural Sciences, Comenius University in Bratislava, Ilkovičova 6, 842 15 Bratislava, Slovak Republic

² Department of Nuclear Chemistry, Faculty of Nuclear Sciences and Physical Engineering, Czech Technical University in Prague, Břehová 7, 115 19 Prague, Czech Republic

physical or chemical activation. Physical activation is a two-step process that uses activators such as CO_2 , air, water vapor or their mixtures [15]. However, activated carbon prepared through physical activation is unsuitable as an adsorbent due to its deficits in properties important for efficient adsorption processes [13]. Chemical activation, on the other hand, is a one-step process where activation agents serve as dehydrating and oxidizing agents simultaneously [16]. Chemical activation agents can be divided to acidic, basic and neutral. Acidic activators consist of inorganic acids, such as phosphoric, nitric, sulfuric and hydrochloric acid. Most common basic activators are NaOH and KOH and neutral chemical activators include for instance K_2CO_3 , ZnCl_2 , or CaCl_2 [17]. Some studies have shown that mixtures of activating agents, such as $\text{FeCl}_3/\text{MgCl}_2$ or $\text{FeCl}_3/\text{ZnCl}_2$ are also effective for synthesizing activated carbon [15]. The effectiveness of the activator increases with its addition [3]. Further modifications of prepared materials by activation aim to optimize the surface chemistry for specific adsorbate adsorption, and these modifications fall into four main categories: oxidation, sulfuration, nitrogenation and functionalization with coordination ligands [18].

Concerns about the dangerous effects of ionizing radiation and radionuclides on the environment and humans have led to research on mitigating these effects [19]. Various methods are employed to remove radionuclides from aqueous systems, including phytoremediation [20], ion exchange [21], chemical precipitation [22], liquid extraction [23], reverse osmosis [24], electrochemical purification [25] or adsorption [6].

Activated carbon is utilized in nuclear chemistry and radioecology as an adsorbent of ecotoxicologically significant radionuclides, including technetium, which is present in spent nuclear fuel. Technetium occurs naturally in trace amounts as a result of the spontaneous decay of uranium isotopes [26]. Anthropogenic sources, such as radioactive fallout or releases after the Chernobyl nuclear accident in 1986, also contribute to higher levels of technetium contamination [27]. In the environment, pertechnetate anion is the predominant chemical form of technetium under aerobic conditions. It is known for its good solubility and mobility in aqueous systems. Given the long half-life of ^{99}Tc (211 000 y), substantial efforts are being made to understand the long-term biogeochemical behaviour of this isotope, its transport in food chains and the mechanisms governing its mobility in different environments [28, 29]. $^{99\text{m}}\text{Tc}$, a metastable nuclear isomer of ^{99}Tc with a half-life of nearly 6 h, is widely used in nuclear medicine to localize damaged tissues [30]. Due to its relatively short half-life, this isotope can also be used as a radiotracer for ^{99}Tc [27]. The preparation of $^{99\text{m}}\text{Tc}$ isotope involves the use of a Mo-Tc generator [31] and ^{99}Mo , the precursor, is usually obtained through neutron irradiation of ^{98}Mo or ^{235}U

in a nuclear reactor or during the reprocessing of spent nuclear fuel cells [27, 32]. In the chromatographic column of the generator, ^{99}Mo is adsorbed on an adsorbent, such as Al_2O_3 or activated carbon. Pertechnetate, being monovalent, is not strongly bound and shows limited interaction with the adsorbent. By adding NaCl as an eluent to the column, anion exchange between Cl and Tc ions occurs, leading to the subsequent elution of a colorless $\text{Na}^{99\text{m}}\text{TcO}_4$ solution while Mo remains on the column [33]. Technetium can be immobilized by barrier materials, transforming Tc into a less mobile, reduced form Tc(IV) through the use of various reducing agents [34, 35]. Another approach involves using barrier clay materials modified with quaternary amines. This eliminates the need to create reductive conditions during redox processes, thereby simplifying the establishment and operation of radioactive waste sites [36]. Incorporating activated carbons as a modifying additive in barrier materials emerges as a promising strategy for technetium immobilization. A critical consideration in adopting this approach is determining the feasibility of seamlessly integrating the additive into the barrier material without compromising its strength and permeability characteristics. Additionally, it is imperative to ensure that the immobilization capacity of the additive remains high within the specified volume provided by the barrier material [34]. The adsorption of pertechnetate has been investigated using a variety of adsorbents. Activated carbon [36–40], along with other inorganic adsorbents such as metallic minerals [41–45] and sulfur-based materials [46, 47], has been studied extensively. Organic adsorbents, including porous polymers, covalent-organic frameworks, metal-organic frameworks, and resins, have also been explored [48]. Biological adsorbents, such as biopolymers like chitosan, cellulose, and chitin, have recently shown promise in pertechnetate adsorption [49–51]. Each of these groups has its own set of advantages and disadvantages. Inorganic adsorbents remain valid in adsorption experiments conducted in the nuclear industry due to their low cost, mechanical strength, various possible modification, and ease of preparation. Organic adsorbents, on the other hand, are more challenging to prepare and tend to be more expensive, making them less practical. Biosorbents are gaining popularity, but their effectiveness in pertechnetate adsorption is still extensively under study [48].

The focus of this study was to characterize new activated carbon samples prepared from fibrous cellulose using different chemical activating agents and compare their adsorption behaviour towards pertechnetate anion with other activated carbon samples prepared from the same precursor, as previously described in scientific papers [40, 52–54]. The study investigated the influence of the initial pH of the solution, contact time of the phases,

and concentration of the adsorbate using adsorption isotherm models (Langmuir and Freundlich).

Materials and methods

Materials

The AC samples were prepared at the Institute of Polymers SAV by researchers Novák & Berek. Comprehensive information regarding the preparation and treatment specifics for each sample can be accessed in Table 1. All chemicals used in this study were of analytical grade and supplied from SLAVUS, s.r.o., Bratislava, Slovak Republic, except for carrier chemical of Tc (NH_4ReO_4), which was supplied from Sigma-Aldrich, Saint Louis, MO, USA. Technetium in the form of $[\text{}^{99\text{m}}\text{Tc}]\text{NaTcO}_4$ was eluted using 0.9% solution of NaCl, directly from ^{99}Mo - $^{99\text{m}}\text{Tc}$ Ultra-Technekow FM generator provided from Oncological Institute of St. Alžbeta, s.r.o., Bratislava, Slovak Republic.

The pyrolysis lasted for 1 h, and the drying occurred at 110 °C.

Characterization

Various characterization techniques were used to study of the AC samples. The specific surface area value for each sample was determined using the BET isotherm analysis. The quality of functional groups on the AC samples surface was investigated using Fourier-transform infrared spectroscopy (FTIR) with the organic oil Nujol method. Sample was combined with the oil on a watch glass until a suspension was formed which we applied to the glass. FTIR spectra were measured by spectrometer NICOLET 6700—Thermo scientific, USA. Measurements were performed at room temperature. X-ray diffraction analysis (XRD) was performed using the Miniflex600 (Rigaku, Tokyo, Japan) instrument to examine the structural properties of the samples. Measurement parameters were as

follows: tension on the X-ray 40 kV, electric current 15 mA, angle range 3–80°, speed 5° min⁻¹. The sample was placed on a slide glass and then covered with a coverslip. The coverslip was then removed and the sample was placed in the instrument holder. X-ray fluorescence analysis (XRF) with a NITON LX3t Analyzer spectrometer with GOLDD Technology (Thermo Scientific, USA) was used for elemental identification. A thin foil (4 μm) was placed on one side of the plastic circle. The outer ring was used to stretch the foil and secure it to the ring. The samples were then poured into the attachment and it was placed in the holder above the detector. High-resolution electron microscopy was used to analyze the structure of the samples. Characterization using this method was carried out at the Department of Ecochemistry and Radioecology FPV UCM in Trnava. Before SEM–EDX analysis, the samples were incubated for 4 h in 0.5 mol·dm⁻³ CaCl₂, dried for 72 h at 45 °C, and the samples were fixed on an aluminum substrate using Ag-adhesive. The samples were subsequently plated with Au using a BP 343,7 (TESLA ELMI). Images were taken using a VEGA 2 SEM microscope (TESCAN) with an EDX QUANTAX QX2 microprobe (RONTec). One image was selected from each new AC sample, which was used for this study. Images were taken at 200x, 500x, 1000x and 3000x magnification. The analysis was performed at a pressure of 36·10⁻³ Pa and voltage of 30 kV. In this study, we used an image with a 500x magnification, which was the most suitable of all, due to the better mapping of the individual elements of the activation process.

Adsorption experiments

To evaluate the adsorption experiments, the following mathematical equations were used:

$$n = \frac{N}{t} [\text{s}^{-1}] \quad (1)$$

Table 1 Preparation and treatment of AC samples

Sample	Preparation and treatment
A-CF-F	Fibrous cellulose, Fe(OH) ₃ , pyrolysis at 700 °C, washing, drying
A-CF-Z	Fibrous cellulose, pyrolysis at 600 °C, then deposited ZnO (precipitated from the solution as Zn(OH) ₂ and converted to ZnO by heating at 400 °C
AC-A	Fibrous cellulose, pyrolysis at 700 °C, washing, drying
AC-B	Fibrous cellulose, 20% ZnCl ₂ , drying, pyrolysis at 530 °C, washing, drying
AC-C	Fibrous cellulose, pyrolysis at 530 °C, warm ethanol solution of H ₃ BO ₃ , drying, washing with ethanol, drying, washing
AC-E	Fibrous cellulose, pyrolysis at 530 °C, 10% FeCl ₃ + drops of 10% NH ₃ (l), filtration, washing, drying
AC-SC	Commerce sample SEPARCOL, CARB-Seal, IMC-T-00-00003-Upo
AC-F	AC-SC sample, 15 min boiling with HNO ₃ , washing, drying
AC-G	AC-SC sample, 15 min boiling with Na ₂ S ₂ O ₅ , washing, drying

$$\sigma_p = \sqrt{(\sigma_{np+f})^2 + (-\sigma_{n_f})^2} [s^{-1}] \quad (2)$$

$$\sigma_{n_s} = \sqrt{(\sigma_{n_{s+f}})^2 + (-\sigma_{n_f})^2} [s^{-1}] \quad (3)$$

$$R = 100 - \left(\frac{n_p}{n_s}\right) \cdot 100[\%] \quad (4)$$

$$\sigma_R = \sqrt{\left(-100 \cdot \frac{1}{n_s} \cdot \sigma_p\right)^2 + \left(100 \cdot \frac{n_p}{n_s^2}\right)^2} [\%] \quad (5)$$

$$D_g = BF \cdot \frac{n_s - n_p}{n_p} [ml \cdot g^{-1}] \quad (6)$$

$$\sigma_{D_g} = \sqrt{\left(BF \cdot \frac{1}{n_p} \cdot \sigma_s\right)^2 + \left(-BF \cdot \frac{n_s}{n_p^2} \cdot \sigma_p\right)^2} [mol \cdot dm^{-3}] \quad (7)$$

$$c_{eq} = c \cdot \frac{n_p}{n_s} [mol \cdot dm^{-3}] \quad (8)$$

$$\sigma_{c_{eq}} = \sqrt{\left(\frac{c}{n_s} \cdot \sigma_{n_p}\right)^2 + \left(-c \cdot \frac{n_p}{n_s^2}\right)^2} [mol \cdot dm^{-3}] \quad (9)$$

$$Q = D_g \cdot c_{eq} [mmol \cdot g^{-1}] \quad (10)$$

$$\sigma_Q = \sqrt{(c_{eq} \cdot \sigma_{D_g})^2 + (D_g \cdot \sigma_{c_{eq}})^2} [mmol \cdot g^{-1}] \quad (11)$$

$$n_0 = \frac{n_p}{e^{-\lambda \cdot t_0}} [s^{-1}] \quad (12)$$

where n is counts per second (index p is sample, index s standard), N is the number of counts shown on the detector, R is the adsorption percentage, D_g is the mass distribution ratio, BF is the batch factor, c_{eq} is the equilibrium concentration, Q is the adsorbed amount, n_0 is the corrected counts per second for the half-life of ^{99m}Tc , t_0 is the corrected time, which passes between measuring the blank sample and the other samples, and σ represents the corresponding uncertainty for each value.

The adsorption experiment of pertechnetate on AC samples were performed using the radioisotope indication method with a radioisotope ^{99m}Tc , with the final volume activity of $1 \text{ MBq} \cdot \text{cm}^{-3}$. Batch adsorption was performed under aerobic conditions at room temperature. The batch factor used in this study was $BF = 100 \text{ cm}^3 \cdot \text{g}^{-1}$.

Using a RADWAG AS 220 R2, Poland, 50 mg of sample was weighed into a plastic test tube with a volume of 10 ml and 5 ml of aqueous phase was then added. AC sample and aqueous phase were mixed in a Programmable laboratory Rotator-Mixer, Biosan Multi Bio RS-24 with a constant mixing time (30 rpm). After the adsorption process took place, the suspension was filtrated using a filtrating paper, 5 ml plastic tip and a compressor. An aliquot of each supernatant was collected and analyzed with a scintillation detector NaI(Tl) using a single-channel amplitude analyzer NP-420. Subsequently, the results were compared with those of the standard (blank) solution. The number of counts on the NaI(Tl) detector was corrected based on the half-life of ^{99m}Tc for each sample and blank measurement. The effect of initial pH of the solution was analyzed between pH 0–8. The pH value of the solutions was adjusted with diluted solutions of HCl and NH_3 with an analytical concentration of 0,1 mol/l on a pH meter HI 2215 pH/ORP (Hanna Instruments). The influence of contact time was studied between 1 and 60 min. Adsorption isotherm studies were carried out using a carrier solution of NH_4ReO_4 , with different initial analytical concentration: $1 \cdot 10^{-5} \text{ mol} \cdot \text{dm}^{-3}$, $5 \cdot 10^{-5} \text{ mol} \cdot \text{dm}^{-3}$, $1 \cdot 10^{-4} \text{ mol} \cdot \text{dm}^{-3}$, $5 \cdot 10^{-4} \text{ mol} \cdot \text{dm}^{-3}$, $1 \cdot 10^{-3} \text{ mol} \cdot \text{dm}^{-3}$, $5 \cdot 10^{-3} \text{ mol} \cdot \text{dm}^{-3}$, $1 \cdot 10^{-2} \text{ mol} \cdot \text{dm}^{-3}$, $5 \cdot 10^{-2} \text{ mol} \cdot \text{dm}^{-3}$ and $1 \cdot 10^{-1} \text{ mol} \cdot \text{dm}^{-3}$. Langmuir isotherm represents a theoretical model that assumes monolayer adsorption. The mathematical description of the Langmuir adsorption model is as follows:

$$c_s = \frac{cs_{max} \cdot b \cdot c_{eq}}{(1 + b \cdot c_{eq})} [mmol \cdot g^{-1}] \quad (13)$$

c_s represents adsorption capacity, c_{eq} is the equivalent concentration, cs_{max} is maximum adsorption capacity, which corresponds to the saturation of sites and b is the ratio of the rate constant of adsorption and desorption.

The Freundlich isotherm is a model that describes ideal and reversible adsorption that is not limited to monolayer formation. This isotherm is valid for low degrees of surface coverage. The Freundlich isotherm can be described by the following mathematical relation:

$$q_F = k_F \cdot c_{eq}^{n_F} [mmol \cdot g^{-1}] \quad (14)$$

k_F is the Freundlich constant, n_F is regression constant and c_{eq} is the equilibrium concentration.

Langmuir and Freundlich adsorption isotherm models were used in this manuscript because they are commonly employed to describe the adsorption process of various activated carbon and biochar samples [48, 55–57].

In this particular study, the recovery of pertechnetate was not investigated. However, recovery could be achieved through several processes, including desorption with

eluent, the use of competing anions with higher affinity towards the materials, temperature changes, sequential washing, or on sulfide minerals such as pyrite [34, 47, 54].

Results and discussion

Characterization of AC samples

Figure 1 shows the specific surface area values of individual AC samples. A higher specific surface area value typically correlates with enhanced adsorbent efficiency for the intended application. The S_{BET} values of AC samples decreased in the order AC-G > A-CF-Z > AC-B > AC-F > AC-SC > AC-C > A-CF-

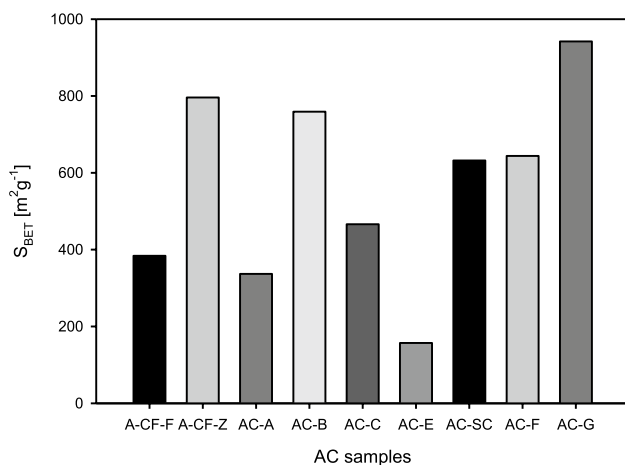


Fig. 1 Specific surface area values for AC samples

F > AC-A > AC-E. These values depend on the preparation process, raw material and activating agent. Notably, all samples underwent chemical activation for their preparation. Samples derived from fibrous cellulose displayed a positive response to activation with Zn compounds (as seen in A-CF-Z and AC-B), while lower values were observed in samples activated with Fe compounds (A-CF-F and AC-E).

Overall, the vibration bands detected in AC samples were of modest intensity, proving indicative assignments. The presence of similar functional groups as observed in other samples from the comparative series can be assumed. FTIR spectra for sample A-CF-F and A-CF-Z are shown in Figs. 2 and 3, respectively. The attribution of specific functional groups to vibration bands for samples A-CF-F and A-CF-Z is detailed in Table 2. A noteworthy difference between the spectra lies in the rounded peak at 1591 cm^{-1} in the sample A-CF-Z, a feature less pronounced in sample A-CF-F. In both cases, the presence of a C=C functional group, characteristic of aromatic rings, was presumed.

XRD spectra are displayed in Figs. 4 and 5. The spectrum of sample A-CF-F lacks distinct identifiable structures, likely due to the abundant presence of iron in the sample. In contrast, the A-CF-Z sample exhibits peaks corresponding to ZnO, $\text{Ca}(\text{CO}_3)_2$, and a compound featuring the simonkolleite structure $\text{Zn}_5(\text{OH})_8\text{Cl}_2 \cdot \text{H}_2\text{O}$.

The summary of identified elements using XRF method are presented in Table 3. In sample A-CF-F, elements Fe, C, Ar, Zn, Ni, Sr, and Ag were present, with the background representing the tube's construction material (Fe, Ni, and W). Sample A-CF-Z contained elements Fe, Ca, Ar, Zn, Ni, Sr, Cl, and Ag, alongside background elements from the tube. All of the identified elements are of macro- and microbiogenic character; therefore, they were obtained from

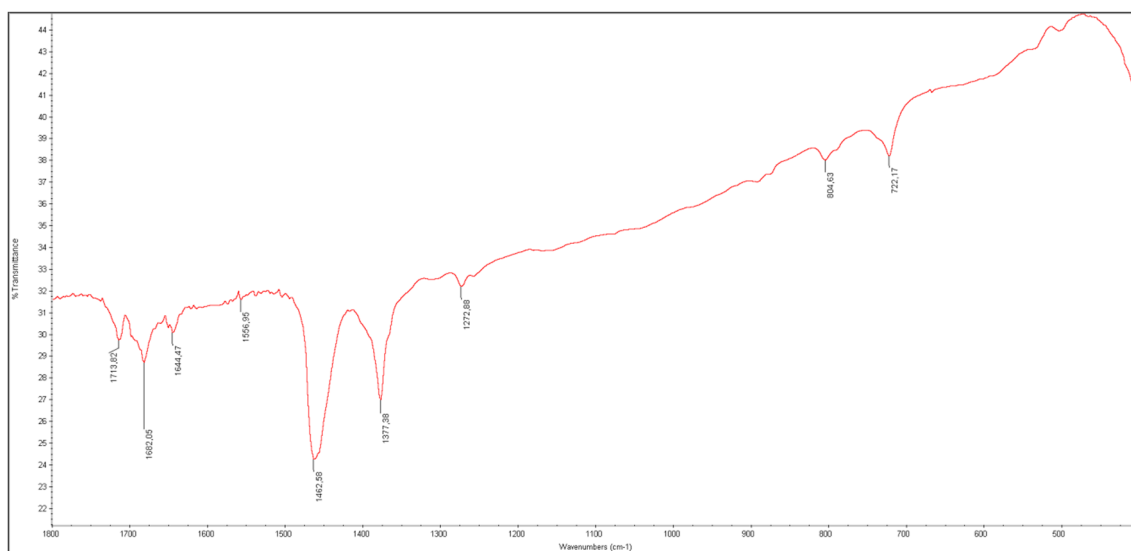


Fig. 2 FTIR spectrum of A-CF-F sample

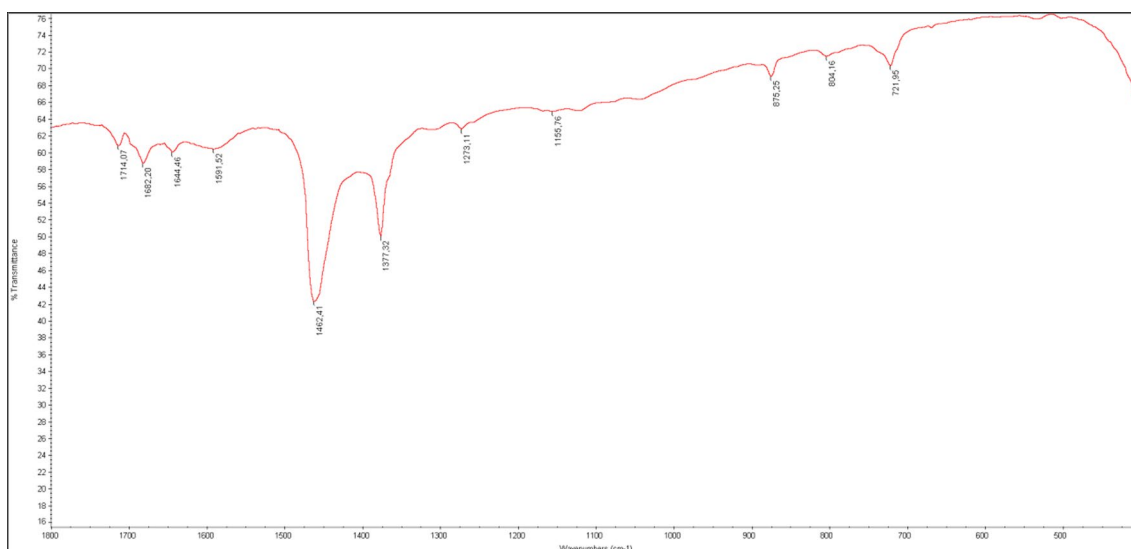


Fig. 3 FTIR spectrum of A-CF-Z sample

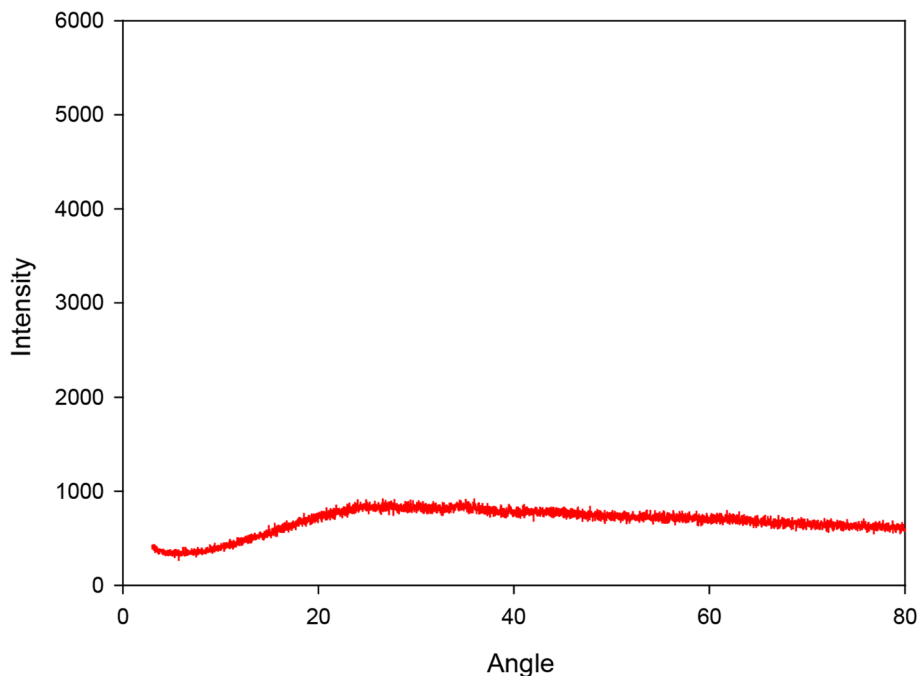
Table 2 Functional groups assigned to the wavenumbers in cm^{-1} of the AC samples

Functional group	A-CF-F	A-CF-Z
–OH	–	–
C=O	1713,1682	1714,1682
C=C	1556	1591
C–H	1462	–
HC=CH	–	–
C–O	1272	1155
C–H vibrations	722,804	721,804,875

outdoor environment, and the plant incorporates them into its metabolism. The XRF method provided information about elements from Al – W; however, for identifying lighter elements, the EDX method was used.

The SEM–EDX method visually confirmed the efficiency of chemical activation in the AC samples and further revealed the presence of Fe and Zn elements in the samples. Figure 6 and 7 showcase the EDX spectrum of each sample's fiber under SEM at 3 000 \times magnification. In each case, a distinct peak corresponding to the constituent elements was visible (Fe, Zn), along with peaks corresponding

Fig. 4 Diffractogram of sample A-CF-F



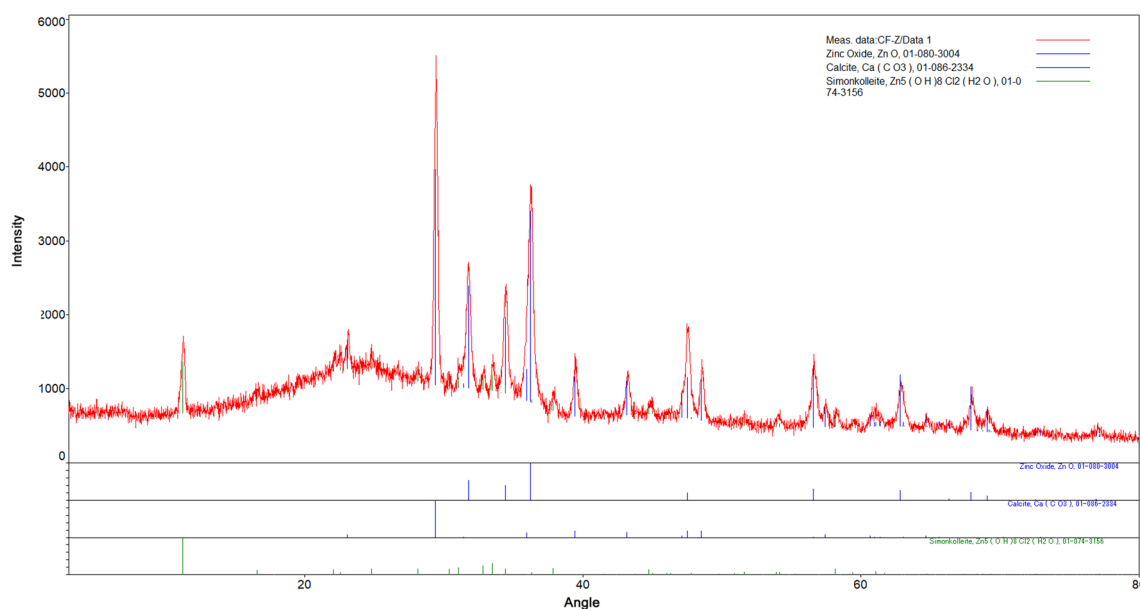


Fig. 5 Diffractogram of sample A-CF-Z

Table 3 Element identification of the AC samples with XRF method

Element	A-CF-F	A-CF-Z
Fe	x	x
Ca	x	x
Ar	x	x
Zn	x	x
Ni (construction)	x	x
Sr	x	x
Ag	x	x
W (construction)	x	x
Cl		x

to other elements, such as Cl, C, Ca, O, Mg, Al, Si, S and Na. Other elements with percentual abundance below 1% can be presumed as microcomponents. Surface mappings of the activation elements, depicted as the electronmicroscopic images in Figures 8 and 9, underscore the uneven distribution of these elements across the samples.

Adsorption experiments

pH of the solution

The dependence of the adsorption percentage R on the initial pH value of the aqueous phase of the studied AC samples is shown in Fig. 10. The A-CF-F sample exhibited notable R values (above 74%) in the acidic pH range of 0 to 4. A significant decline in R (50%) was observed at pH 6, as well as in the alkaline region (pH 8). Higher

pH was not investigated due to preliminary studies, which indicated a significant decrease in the adsorption percentage above pH 8. This observation suggested that higher concentrations of OH^- anions, resulting from an increase in pH, compete for the adsorption of pertechnetate anions on the active sites of the material. Increasing the pH could potentially be used as a desorption method for recovering pertechnetate from activated carbon materials. The adsorption behaviour of pertechnetate on A-CF-F at different pH values closely resembled that of the unactivated AC sample (AC-A). These two samples possess nearly identical specific surface area values. Within the slightly acidic to alkaline pH range, weaker adsorption of Tc was evident, indicating the occurrence of anion desorption. Similar tendencies were observed in the AC-E sample. The A-CF-Z sample displayed elevated R values (more than 94%) across the entire range of investigated pH values (0–8). Likewise, a parallel trend was observed in the AC-B sample, which akin to A-CF-Z, underwent activation with a Zn-containing compound, resulting in closely matched S_{BET} values. pH 2 was judiciously selected as the optimal pH for subsequent batch adsorption experiments on the examined AC samples and is reinforced by the outcomes associated with the AC samples from the same series. With confidence, it can be stated that an initial pH of 2 for the solution guarantees the effective adsorption of pertechnetate across all investigated samples.

Contact time of the solid and liquid phase

The dependence of the adsorption percentage R on the mixing time of the solid and liquid phases of the AC samples is

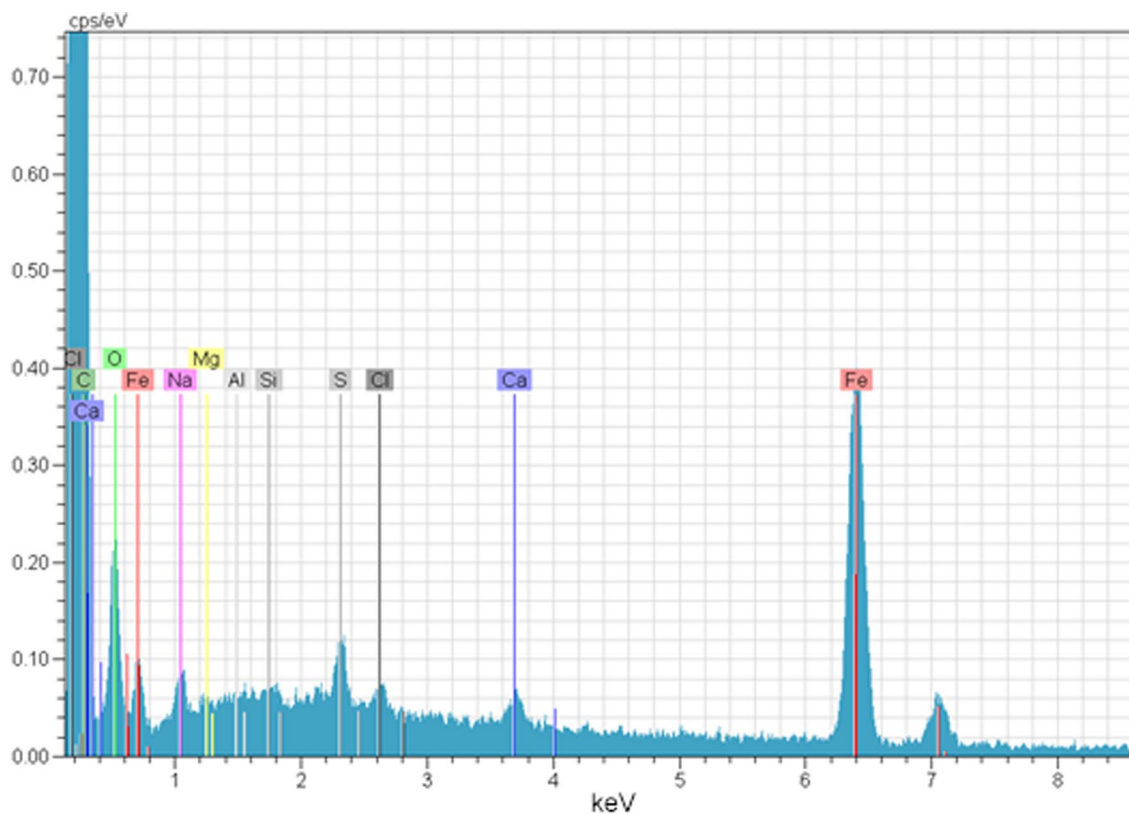


Fig. 6 EDX spectrum of sample A-CF-F

presented in Fig. 11. The A-CF-F sample achieved adsorption equilibrium within 1 h front he initiation of phase mixing. Remarkably, the A-CF-Z sample achieved rapid adsorption equilibrium, accomplishing it withing 1 min of mixing commencement. In contrast, the AC-E sample with the smallest S_{BET} value, attained equilibrium only after 1 h. Consequently, for subsequent batch adsorption experiments, a mixing time of 1 h for the solid and liquid phases was selected. This decision aligns with previous publications showcasing analogous research and is supported by the findings of this study, as well as the preliminary experiments with longer contact time (2 h, 8 h and 24 h).

While certain samples demonstrated swift attainment of high R values in adsorption, others required a full hour to reach equilibrium. It can be confidently stated that all activated carbon samples will efficiently adsorb pertechnetate after 1 h, as evidenced by the elevated R values.

Adsorption isotherms

Figure 12 depicts the Langmuir and Freundlich adsorption isotherms for the examined AC samples, as compared in this article. The adsorption of perrhenate, used as a carrier for pertechnetate, exhibited a decrease as the initial concentration in the solution increased. The computed values

of the adsorbed pertechnetate amount from the Langmuir and Freundlich isotherms closely align with the experimental data. Maximum adsorption capacities (q_{max}) were calculated for each of the activated samples and then compared to some other types of adsorbents, as well as other variations of activated carbons found in the literature (Table 4), with regard to pertechnetate/perrhenate adsorption. When comparing the newly prepared activated carbon samples, the Zn-activated sample performed better, exhibiting the highest q_{max} value among all the samples ($303,03 \text{ mg}\cdot\text{g}^{-1}$). This result aligns with another Zn-activated sample (AC-B), which also showed high adsorption efficiency towards perrhenate.

($q_{\text{max}} = 243,90 \text{ mg}\cdot\text{g}^{-1}$). The inactivated sample had the lowest maximum adsorption capacity. Therefore, it can be said that chemical activation of the AC-A sample through various chemical agents positively influenced the adsorption capacities. The Freundlich adsorption model is deemed more suitable for describing the adsorption of pertechnetate on activated carbon samples in this context. This conclusion is drwan from higher values of the determination coefficient R^2 , as compared between the aforementioned adsorption models (Table 5). Moreover, the higher the value of the determination coefficient, the higher the reproducibility of the results. This suggests that the adsorption process is heterogenous, and the assumption

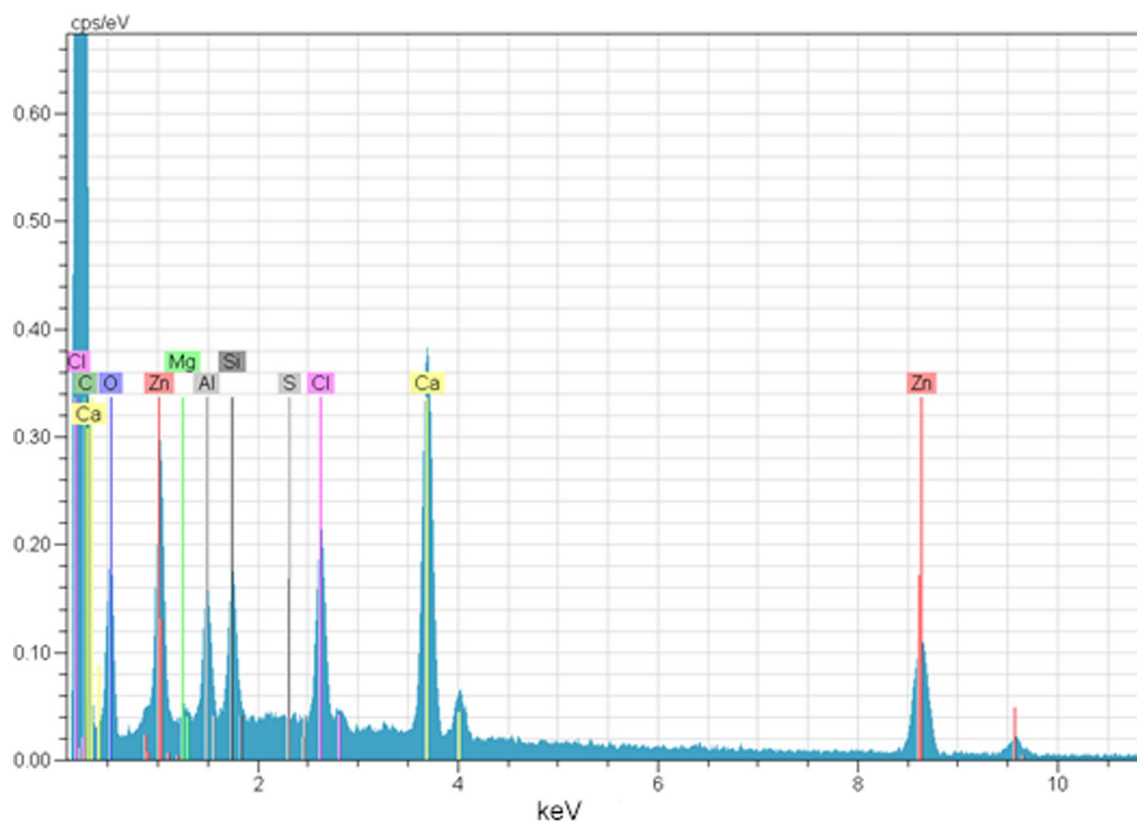


Fig. 7 EDX spectrum of savmple A-CF-Z

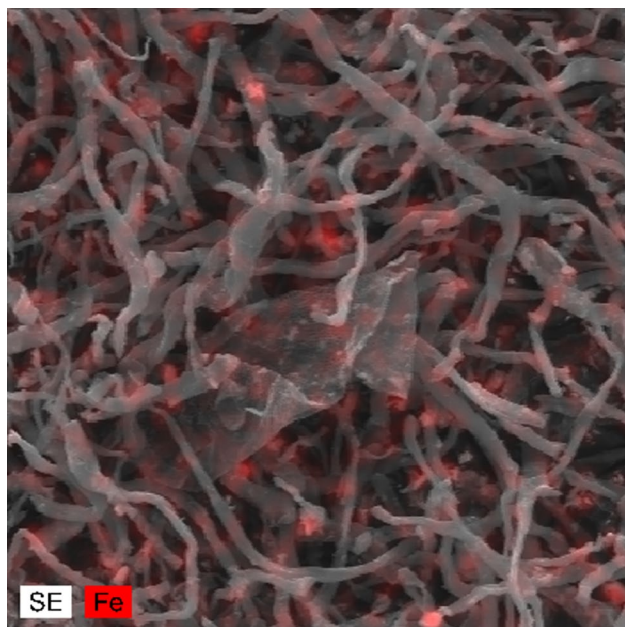


Fig. 8 Electronmicroscopic image of sample A-CF-F

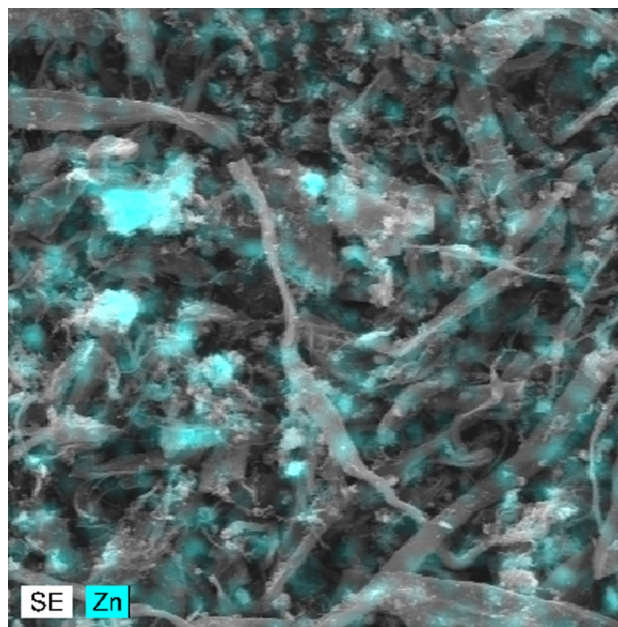


Fig. 9 Electronmicroscopic image of sample A-CF-Z

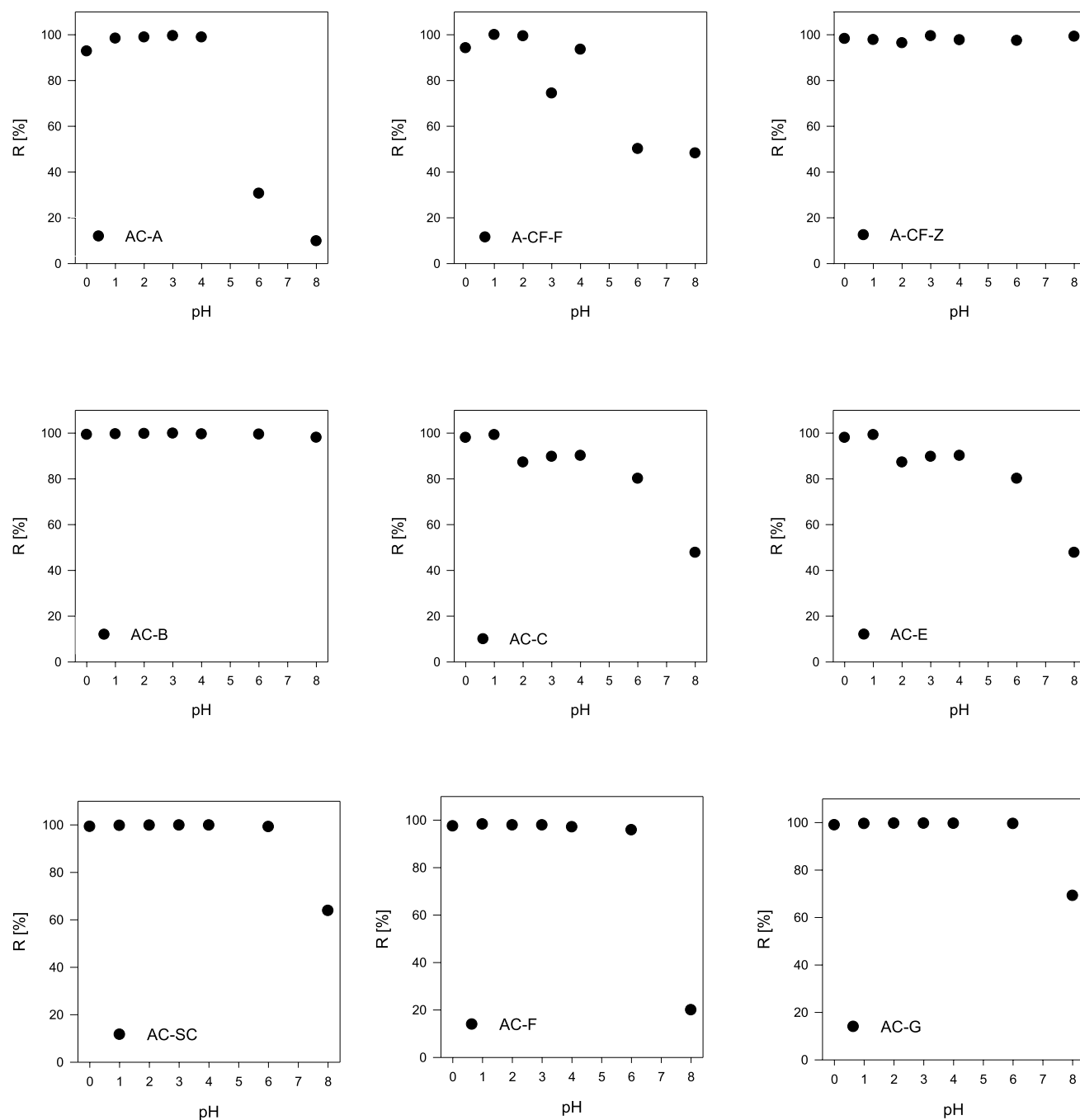


Fig. 10 Influence of initial pH on the adsorption of pertechnetate using AC samples (contact time: 2 h, without carrier, temperature: ambient conditions)

of equal adsorptive sites with constant adsorption heat is not likely [58].

Conclusion

The specific surface area values of individual AC samples depend on the preparation process, raw material and activating agent. The S_{BET} values decreased in the order:

AC-G > A-CF-Z > AC-B > AC-F > AC-SC > AC-C > A-CF-F > AC-A > AC-E. Vibration bands of investigated AC samples were not intense and their assignment was indicative. FTIR and XRD spectra showed similar functional groups. Samples A-CF-F and A-CF-Z contained elements Fe, Ca, Ar, Zn, Ni, Sr and Ag. XRF spectra identified Fe, Ca, Ar, Zn, Ni, Sr, Cl and Ag. SEM-EDX analysis indicated the presence of Fe and Zn elements on the samples, with uneven distribution of activation elements across the surface.

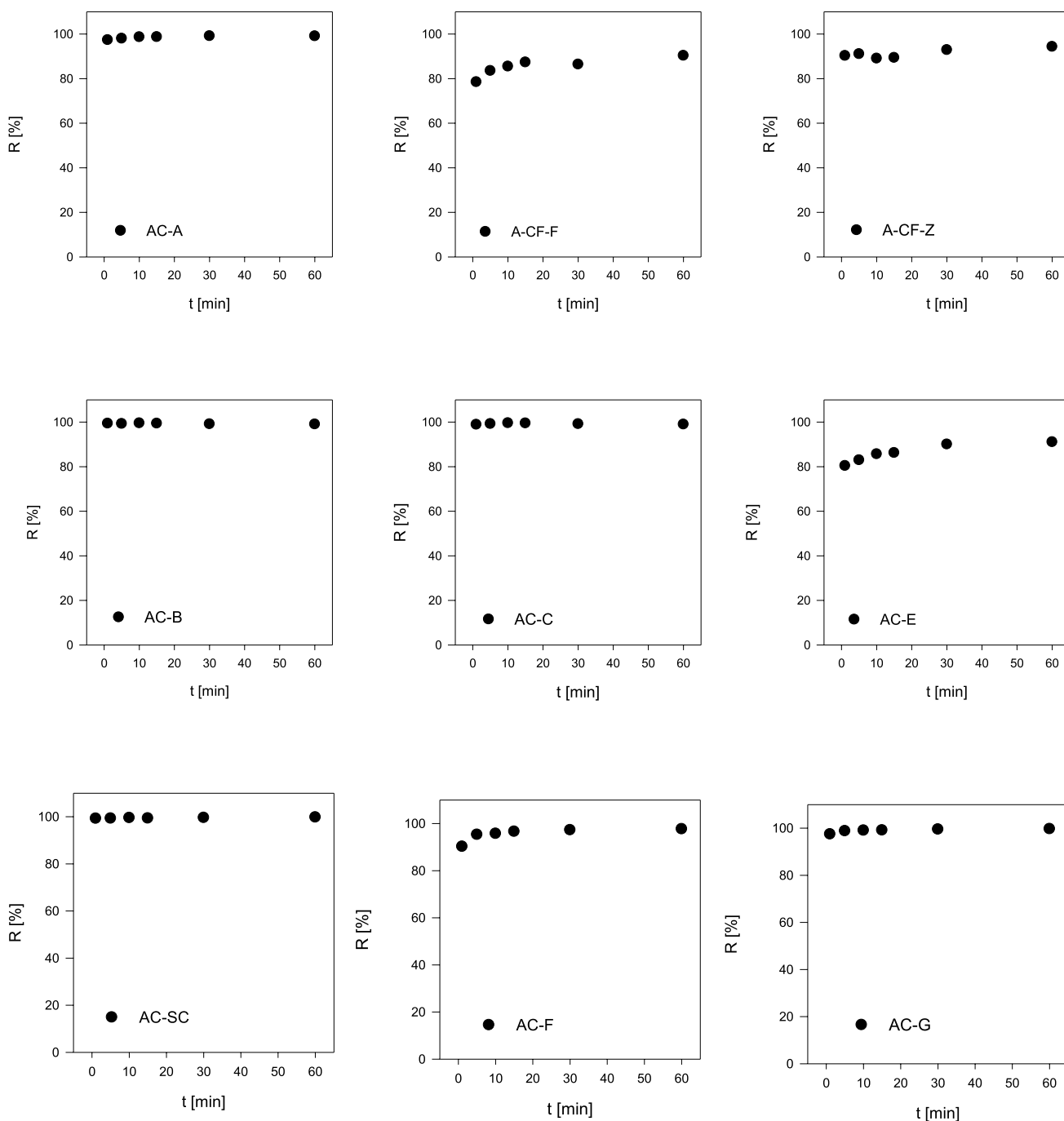


Fig. 11 Influence of contact time on the adsorption of pertechnetate using AC samples (initial pH: 2, without carrier, temperature: ambient conditions)

The A-CF-F sample achieved high R values in the acidic pH range (0–4), while the unactivated AC sample (AC-A) had weaker adsorption in the slightly acidic to alkaline pH range. The A-CF-Z sample achieved high R values in the entire investigated range of pH values (0–8). pH 2 was chosen as the optimal pH for subsequent batch adsorption experiments. The adsorption percentage R of

AC samples relies on the mixing time of solid and liquid phases, with the A-CF-F sample reaching adsorption equilibrium within 1 h and the A-CF-Z sample achieving equilibrium only after 1 h. Pertechnetate adsorption exhibited a decrease with rising initial concentration of the analyte in the solution, with the Freundlich adsorption model proving more suitable for describing pertechnetate adsorption onto

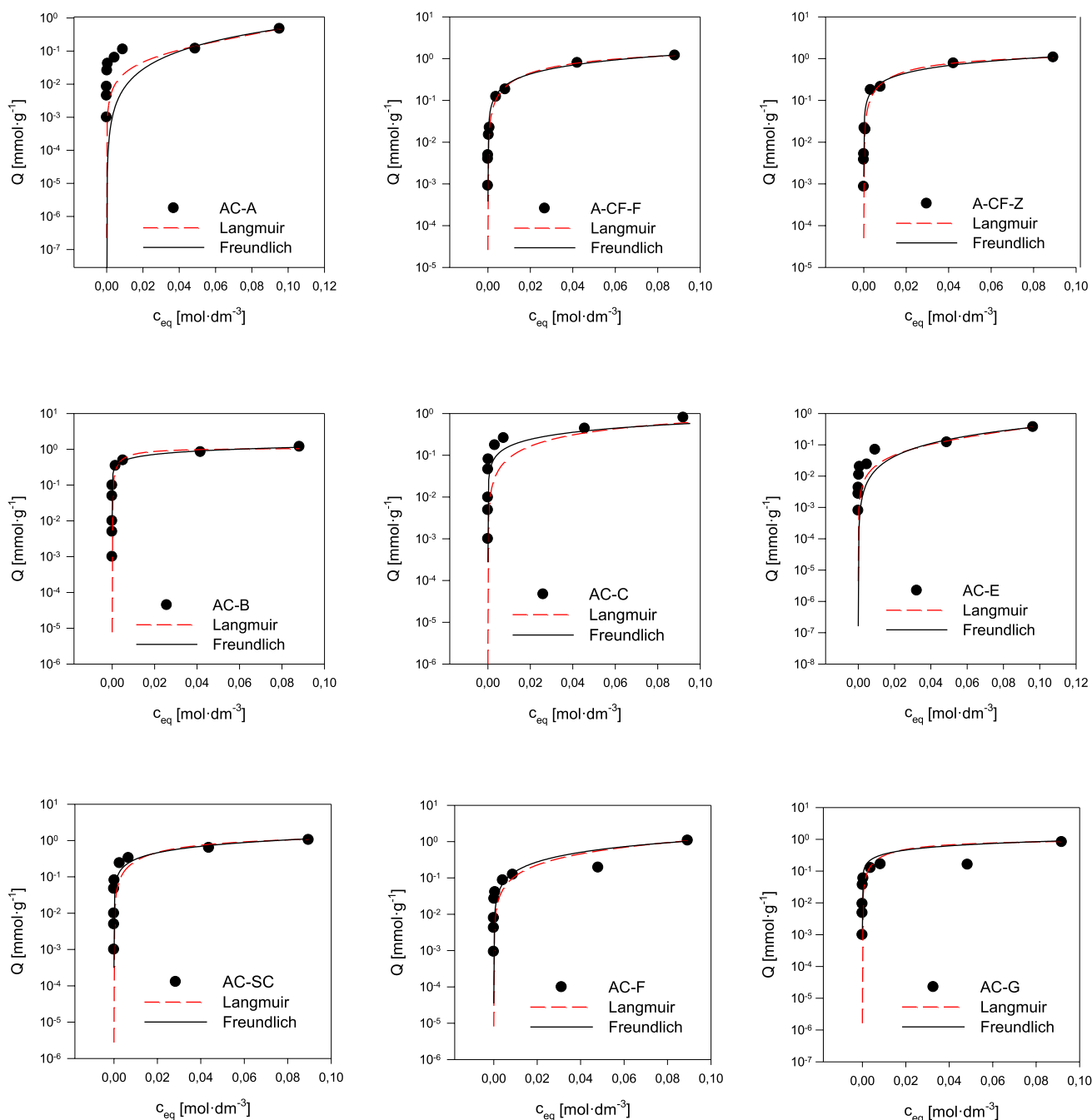


Fig. 12 Adsorption isotherms of AC samples

AC samples, showing better fit when comparing coefficient of determination R^2 . The maximum adsorption capacity calculated from the data was highest for sample A-CF-Z ($303.03 \text{ mg}\cdot\text{g}^{-1}$), followed by a decreasing order: A-CF-F > AC-B > AC-SC > AC-C > AC-F > AC-G > AC-E > AC-A. Consequently, in the comparison of newly prepared samples activated with Zn and Fe compounds, it was observed that the sample activated with Zn compounds exhibited greater efficiency for pertechnetate adsorption,

which also correlates with the adsorption efficiency of the other zinc activated sample, AC-B.

Adsorbents based on activated carbon prepared by pyrolysis of fibrous cellulose effectively adsorb technetium and, thanks to their simple preparation and economic availability, can be used as a suitable alternative to commercially available adsorbents. Chemical activation contributed to elevated specific surface area values and consequently enhanced adsorption properties for technetium

Table 4 Comparison between maximum adsorption capacities of adsorbents

Sample	Maximum adsorption capacity (q_{\max})	References
A-CF-F	285,71 mg•g ⁻¹	This study
A-CF-Z	303,03 mg•g ⁻¹	This study
AC-A	34,60 mg•g ⁻¹	This study
AC-B	243,90 mg•g ⁻¹	This study
AC-C	126,58 mg•g ⁻¹	This study
AC-E	36,90 mg•g ⁻¹	This study
AC-SC	181,81 mg•g ⁻¹	This study
AC-F	7,57 mg•g ⁻¹	This study
AC-G	46,08 mg•g ⁻¹	This study
AC	0,001 mg•g ⁻¹	[59]
GAC 830	27,90 mg•g ⁻¹	[36]
C@PAAGMs	65,64 mg•g ⁻¹	[60]
SDBAC-clinoptilolite	97,30 mg•g ⁻¹	[61]
HDPy-montmorillonite	25,00 mg•g ⁻¹	[45]
PAF-1-F	420,00 mg•g ⁻¹	[62]
SCU-8	126,39 mg•g ⁻¹	[63]

Table 5 Coefficients of determination from fitting the Langmuir and Freundlich isotherms

Sample	Langmuir R ²	Freundlich R ²
AC-A	0.9175 ± 0.04	0.9447 ± 0.05
A-CF-F	0.9942 ± 0.01	0.9991 ± 0.01
A-CF-Z	0.9900 ± 0.04	0.9943 ± 0.03
AC-B	0.9517 ± 0.09	0.9938 ± 0.03
AC-C	0.9556 ± 0.03	0.9675 ± 0.02
AC-E	0.7333 ± 0.11	0.7788 ± 0.11
AC-SC	0.9608 ± 0.08	0.9726 ± 0.06
AC-F	0.8782 ± 0.13	0.8869 ± 0.13
AC-G	0.6787 ± 0.20	0.7331 ± 0.18

in the anionic form. These materials could potentially undergo further modifications to selectively adsorb pertechnetate, or other important radionuclides present in the spent nuclear fuel, particularly within the barriers employed in the back-end of the nuclear fuel cycle.

Acknowledgements This study was supported by the Operation Program of Integrated Infrastructure for the project, UpScale of Comenius University Capacities and Competence in Research, Development and Innovation, ITMS2014+: 313021BUZ3, and Agency of the Ministry of Education, Science, Research and Sport of the Slovak Republic and Slovak Academy of Sciences VEGA Project No. 1/0356/23. Additionally, the study was supported by the Ministry of Education Youth and Sports, project “Center for advanced applied science,” No. CZ.02.1.0 1/0.0/0.0/16_019/0000778—Ultra-trace isotope research in social and environmental studies using accelerator mass spectrometry.

Funding Open access funding provided by The Ministry of Education, Science, Research and Sport of the Slovak Republic in cooperation with Centre for Scientific and Technical Information of the Slovak Republic.

Declarations

Conflict of interest The authors declare that they have no known competing financial interests or personal relationships that could have appeared to influence the work reported in this paper.

Data availability All data generated or analysed during this study are included in this published article.

Open Access This article is licensed under a Creative Commons Attribution 4.0 International License, which permits use, sharing, adaptation, distribution and reproduction in any medium or format, as long as you give appropriate credit to the original author(s) and the source, provide a link to the Creative Commons licence, and indicate if changes were made. The images or other third party material in this article are included in the article's Creative Commons licence, unless indicated otherwise in a credit line to the material. If material is not included in the article's Creative Commons licence and your intended use is not permitted by statutory regulation or exceeds the permitted use, you will need to obtain permission directly from the copyright holder. To view a copy of this licence, visit <http://creativecommons.org/licenses/by/4.0/>.

References

- Schanz JJ, Parry RH (1962) The activated carbon industry. *Ind Eng Chem* 54(12):24–28.
- Xu W, Segall ML, Li Z (2020) Reactivity of Pyrogenic Carbonaceous Matter (PCM) in mediating environmental reactions: current knowledge and future trends. *Front Environ Sci Eng* 14:1–11
- Hagemann N et al (2018) Activated carbon, biochar and charcoal: linkages and synergies across pyrogenic carbon's ABC s. *Water* 10(2):182.
- Alkhatib AJ, Al Zailaey K (2015) Medical and environmental applications of activated charcoal. *Eur Sci J* 11(3):1–7
- Siyal AA, Shamsuddin MR, Low A et al (2020) A review on recent developments in the adsorption of surfactants from wastewater. *J Environ Manage* 254:109797
- Ambaye TG, Vaccari M, Van Hullenbusch ED et al (2021) Mechanisms and adsorption capacities of biochar for the removal of organic and inorganic pollutants from industrial wastewater. *Int J Environ Sci Technol* 18:3273–3294
- Lamaming J, Saalah S, Yaser A et al (2022) A review on bamboo as an adsorbent for removal of pollutants for wastewater treatment. *Int J Chem Eng.*
- Togibasa O, Mumfajjah M, Allo YK et al (2021) The effect of chemical activating agent on the properties of activated carbon from sago waste. *Appl Sci* 11(24):11640
- Al-Othman ZA, Ali R, Naushad M et al (2012) Hexavalent chromium removal from aqueous medium by activated carbon prepared from peanut shell: Adsorption kinetics, equilibrium, and thermodynamic studies. *Chem Eng J* 184:238–247
- Mahamad MN, Zaini MAA, Zakaria ZA et al (2015) Preparation and characterization of activated carbon from pineapple waste biomass for dye removal. *Int Biodeterior Biodegrad* 102:274–280
- Arami-Niya A, Daud WMAW, Mijalli FS et al (2010) Using granular activated carbon prepared from oil palm shell by ZnCl₂ and physical activation for methane adsorption. *J Anal Appl Pyrolysis* 89(2):197–203

12. Rufford TE, Hulicova-Jurcakova D, Zhu Z et al (2008) Nanoporous carbon electrode from waste coffee beans for high performance supercapacitors. *Electrochem Commun* 10(10):1594–1597
13. Tadda MA, Ahsan A, Shitu A et al (2016) A review on activated carbon: process, application and prospects. *J Adv Civil Eng Practice Res* 2(1):7–13
14. Rodriguez JA, Lustosa Filho JF, Melo LCA et al (2020) Influence of pyrolysis temperature and feedstock on the properties of biochars produced from agricultural and industrial wastes. *J Anal Appl Pyrolysis* 149:104839
15. Bedia J, Penas-Garzón M, Goméz-Aviléz A et al (2020) Review on activated carbons by chemical activation with FeCl₃. *J. Carbon Res* 6(2):21
16. Swiatkowski A (1999) Protection, adsorption and its applications in industry and environmental protection. studies in surface science and catalysis
17. Ho SM (2022) A review of chemical activating agent on the properties of activated carbon. *Int J Chem Res* 1:1–13
18. Rivera-Utrilla J, Sanchez-Polo M, Álvarez PM et al (2011) Activated carbon modifications to enhance its water treatment applications: an overview. *J Hazard Mater* 187(1–3):1–12
19. Kusumkar V, Galamboš M, Viglašová E et al (2021) Ion-imprinted polymers: synthesis, characterization, and adsorption of radionuclides. *Materials*.
20. Mahar A, Wang P, Ali A et al (2016) Challenges and opportunities in the phytoremediation of heavy metals contaminated soils: a review. *Ecotoxicol Environ Saf* 126:111–121
21. Kononova ON, Bryuzgina GL, Apchitaeva OV et al (2019) Ion exchange recovery of chromium (VI) and manganese (II) from aqueous solutions. *Arab J Chem* 12(8):2713–2720
22. Mollah A, Begum A, Rahman M et al (1998) Removal of radionuclides from low level radioactive liquid wastewater by precipitation. *J Radioanal Nucl Chem* 229:187–189
23. Khani MH, Keshtkar AR, Ghannadi M, Pahlavanzadeh H (2008) Equilibrium, kinetic and thermodynamic study of the biosorption of uranium onto *Cystoseria indica* algae. *J Hazard Mater* 150(3):612–618
24. Montaña M, Camacho A, Serrano I et al (2013) Removal of radionuclides in drinking water by membrane treatment using ultrafiltration, reverse osmosis and electrodialysis reversal. *J Environ Radioact* 125:86–92
25. Abdi S, Nasiri M, Mesbahi A et al (2017) Investigation of uranium (VI) adsorption by polypyrrole. *J Hazard Mater* 332:132–139
26. L'annunziata MF (2016) Radioactivity: Introduction and History, from the quantum to quarks, 2nd edn. Elsevier, New York
27. Lehto J, Hou X (2011) Chemistry and analysis of radionuclides laboratory techniques and methodology. Wiley, New York
28. Schwochau K (2000) Technetium chemistry and radiopharmaceutical applications. Wiley-VCH, New York
29. Dong Z, Liu J, Wen D et al (2022) Aminomethylpyridine isomers functionalized cellulose microspheres for TcO₄⁻/ReO₄⁻ uptake: structure-properties relationship and their application in different aquatic systems. *J Hazard Mater* 433:128728
30. Peacock VRD (1965) The chemistry of technetium and rhenium. Elsevier, New York
31. Zolle I (2007) Technetium-99m pharmaceuticals. Springer, Cham
32. Kónya J, Nagy NM (2012) Nuclear and radiochemistry, 1st edn. Elsevier, New York
33. Hasan S, Prelas MA (2020) Molybdenum-99 production pathways and the sorbents for ⁹⁹Mo/^{99m}Tc generator systems using (n, γ) ⁹⁹Mo: a review. *SN Appl Sci* 2(11):1782
34. Makarov A, Safonov A, Sitanskaia A et al (2022) Clay and carbon materials-based engineered barriers for technetium immobilization. *Progress Nuclear Energy* 152:104398
35. Pearce CI, Moor RC, Morad JW et al (2020) Technetium immobilization by materials through sorption and redox-driven processes: a literature review. *Sci Total Environ* 716:132849
36. Li D, Seaman JC, Kaplan DI et al (2019) Per technetate (TcO₄⁻) sequestration from groundwater by cost-effective organoclays and granular activated carbon under oxic environmental conditions. *Chem Eng J* 360:1–9
37. Gu C, Huang N, Chen Y et al (2016) Porous organic polymer films with tunable work functions and selective hole and electron flows for energy conversion. *Angew Chem* 55(9):3049–3053
38. Rajec P, Galamboš M, Daňo M et al (2015) Preparation and characterization of adsorbent based on carbon for per technetate adsorption. *J Radioanal Nucl Chem* 303:277–286.
39. Popova NN, Bykov LG, Petuhova GA et al (2012) A study of physicochemical properties of modified carbon nanomaterials intended for sorption extraction of radionuclides I. The influence of the porosity of carbon nanomaterials on their sorption properties with respect to Tc(VII). *Protect Met Phys Chem Surface* 48(6):665–670
40. Daňo M, Viglašová E, Galamboš M et al (2017) Sorption behaviour of per technetate on oxidized and reduced surface of activated carbon. *J Radioanal Nucl Chem* 314:2219–2227
41. Peretyazhko T, Zachara JM, Heald SM et al (2008) Reduction of Tc(VII) by Fe(II) sorbed on Al (hydr) oxides. *Environ Sci Technol* 42(15):5499–5506
42. Um W, Chang HS, Icenhower JP et al (2011) Immobilization of 99Technetium (VII) by Fe(II)-goethite and limited reoxidation. *Environ Sci Technol* 45(11):4904–4913
43. Liu J, Pearce CI, Qafoku O et al (2012) Tc(VII) reduction kinetics by titanomagnetite (Fe_{3-x}Ti_xO₄) nanoparticles. *Geochem Cosmochim Acta* 92:67–81
44. Lee MS, Saslow SA, Um W et al (2020) Impact of Cr and Co on Tc-99 retention in magnetite: a combined study of ab initio molecular dynamics and experiments. *J Hazard Mater* 387:121721
45. Luo W, Inoue A, Hirajima T et al (2017) Synergistic effect of Sr²⁺ and ReO₄⁻ adsorption on hexadecyl pyridinium-modified montmorillonite. *Appl Surf Sci* 394:431–439
46. Watson JHP, Croudace IW, Warwick PE et al (2001) Adsorption of radioactive metals by strongly magnetic iron sulfide nanoparticles produced by sulfate-reducing bacteria. *Separ Sci Technol* 36(12):2571–2607
47. Rodríguez DM, Mayordomo N, Scheinost AC et al (2020) New insights into Tc-99(VII) removal by pyrite: a spectroscopic approach. *Environ Sci Technol* 54(5):2678–2687
48. Wang J, Xu B (2023) Removal of radionuclide 99Tc from aqueous solution by various adsorbents: a review. *J Environ Radioact* 270:107267
49. Pivarciova L, Rosskopfova O, Galamboš M et al (2016) Sorption of per technetate anions on chitosan. *J Radioanal Nucl Chem* 308(1):93–98
50. Pivarciova L, Rosskopfova O, Galamboš M et al (2016) Sorption of technetium on glutaraldehyde crosslinked chitosan. *J Radioanal Nucl Chem* 309(3):1251–1256
51. Zhang H, Yang F, Lu C et al (2020) Effective decontamination of (TcO₄⁻)-Tc-99/ReO₄⁻ from Hanford low-activity waste by functionalized graphene oxide-chitosan sponges. *Environ Chem Lett* 18(4):1379–1388
52. Daňo M (2020) Štúdium sorpcie technecistanu na uhlíkatých materiáloch (Diss. thesis). ČVUT, Prague
53. Galamboš M, Daňo M, Viglašová E et al (2015) Effect of competing anions on per technetate adsorption by activated carbon. *J Radioanal Nucl Chem* 304:1219–1224
54. Viglašová E, Daňo M, Galamboš M et al (2016) Column studies for the separation of ^{99m}Tc using activated carbon. *J Radioanal Nucl Chem* 307:591–597

55. Fidel RB, Laird DA, Spokas KA (2018) Sorption of ammonium and nitrate to biochars is electrostatic and pH-dependent. *Sci Rep* 8:17627
56. Long L, Xue Y, Hu X et al (2019) Study on the influence of surface potential on the nitrate adsorption capacity of metal modified biochar. *Environ Sci Pollut Res* 26:3065–3074
57. Zhou L, Xu D, Li Y et al (2019) Phosphorus and nitrogen adsorption capacities of biochars derived from feedstocks at different pyrolysis temperatures. *Water* 11:1559
58. DeMessie JA, Sorial GA, Sahle-Demessie E (2022) Removing chromium (VI) from contaminated water using a nano-chitosan-coated diatomaceous earth. *Separ Sci Technol* 15:163–176
59. Liang LY, Gu BH, Yin XP (1996) Removal of technetium-99 from contaminated groundwater with sorbents and reductive materials. *Sep Technol* 6(2):111–122
60. Wang K, Chen S, Qiu R et al (2022) Convenient preparation of activated carbon modified phosphoric acid-activated geopolymer microspheres (C@PPAGMs) for the efficient adsorption of ReO_4^- implications for TcO_4^- elimination. *Compos Part B-Eng* 247:110296
61. Milicevic S, Matovic L, Petrovic D et al (2016) Surfactant modification and adsorption properties of clinoptilolite for the removal of pertechnetate from aqueous solutions. *J Radioanal Nucl Chem* 310(2):805–815
62. Banerjee D, Xu WQ, Nie ZM et al (2016) Zirconium-based metal-organic framework for removal of perchlorate from water. *Inorg Chem* 55(17):8241–8243
63. Li Y, Yang ZX, Wang YL et al (2017) A mesoporous cationic thorium-organic framework that rapidly traps anionic persistent organic pollutants. *Nat Commun* 8(1):1354

Publisher's Note Springer Nature remains neutral with regard to jurisdictional claims in published maps and institutional affiliations.